Chapter 2

Ferroelectrics

2.1 Introduction

The first part of this thesis is focused on producing an active MIM waveguide with a ferroelectric layer as the active material. Henceforth, the analysis of ferroelectrics will be done with two materials which acccurately represent the field, barium titanate ($BaTiO_3$) and lithium niobate ($LiNbO_3$). In this chapter, we will introduce ferroelectrics and motivate why these materials present a unique opportunity for use in active plasmonic devices. These materials exhibit a wide range of properties including piezoelectricity, ferroelectricity, pyroelectricity, and electro-optic effects. The intensity of these effects within the materials is directly related to the quality of the crystal in question. As a result, ion implantation induced layer transfer is introduced at the conclusion of this chapter as a method of producing single crystal thin film ferroelectrics.

2.2 Point Groups and Crystal Symmetry

2.2.1 Symmetry

All crystalline materials can be represented by a crystal lattice and a basis. The lattice represents the three-dimensional periodic array of points in space. These points form individual "unit cells" which represent the smallest repeat unit of the lattice. The basis represents the atom or atoms which lie on each point within the lattice. These crystals can be organized by their symmetry operations and divided into 32 distinct "point groups". Of these 32 groups, 11 have a well defined center of symmetry and are defined as centrosymmetric. Out of the remaining 21 groups, 20 are piezoelectric [the (432) point group being the only exception]. Out of the 20 piezoelectric point groups, 10 have a unique polar axis and are referred to as ferroelectric. Below a critical transition temperature, the Curie temperature (T_c), ferroelectric materials exhibit a spontaneous polarization due to a distortion in the crystal structure. A diagram of the different crystal systems is shown in

Figure 2.1, and the piezoelectric point groups are shown in the boxed, grey region.

Polarity	Symmetry	Crystal system										
		Cubic		Hexagonal		Tetragonal		Rhombohedral		Orthorhombic	Monoclinic	Triclinic
Non-polar (22)	Centro (11)	$m\bar{3}m$	$m\bar{3}$	$6/mmm$	$6/m$	$4/mmm$	$4/m$	$\bar{3}m$	$\bar{3}$	mmm	$2/m$	
	Non-centro (21)	$\bar{4}3m$ 432	23	$\bar{6}m2$ 622	$\bar{6}$	$\bar{4}2m$ 422	$\bar{4}$	32		222		
Polar (Pyro-electric) (10)				$6mm$	6	$4mm$	4	$3m$	3	$mm2$	2 m	1

Figure 2.1. Shown here are the 32 crystal point groups. The piezoelectric groups are shown in the boxed, grey region.

2.2.2 Crystal Polarization

The two ferroelectrics that will be studied throughout this thesis are barium titanate ($BaTiO_3$) and lithium niobate ($LiNbO_3$). $BaTiO_3$ is one of the most well studied and widely used ferroelectrics. It belongs to a category of materials called ABO_3 perovskites. Above T_c, these materials have a cubic unit cell and below T_c, they have a tetragonal unit cell, Figure 2.2. In the cubic state, the A atom resides in the center of the unit cell, the B atoms reside on the 8 corners, and the oxygen atoms lie in the 6 face-centered positions. From a physical standpoint, when cubic $BaTiO_3$ is cooled below T_c, there is a contraction along the $\vec{a}$-axis and a corresponding elongation along the $\vec{c}$-axis. As a result, above T_c, the Ba atom sits in the center of the cubic unit cell and is surrounded by the 4 oxygen atoms in the central plane of the unit cell. Upon cooling below T_c, the contraction in the $\vec{a}$-axis results in the oxygen atoms moving towards the center of the unit cell, and this forces the Ba atom to move either above or below the central plane of oxygen atoms, Figure 2.2. This produces the spontaneous polarization that is associated with ferroelectrics. When the crystal is subjected to an external pressure, the crystal structure will realign to relieve this force and as a

result, generate a net electric field. This is the *direct piezoelectric effect*. The converse of this is also true. Under an applied electric field, the unit cell dipoles will realign themselves with the field and change the crystal dimensions. This is known as the *converse piezoelectric effect*.

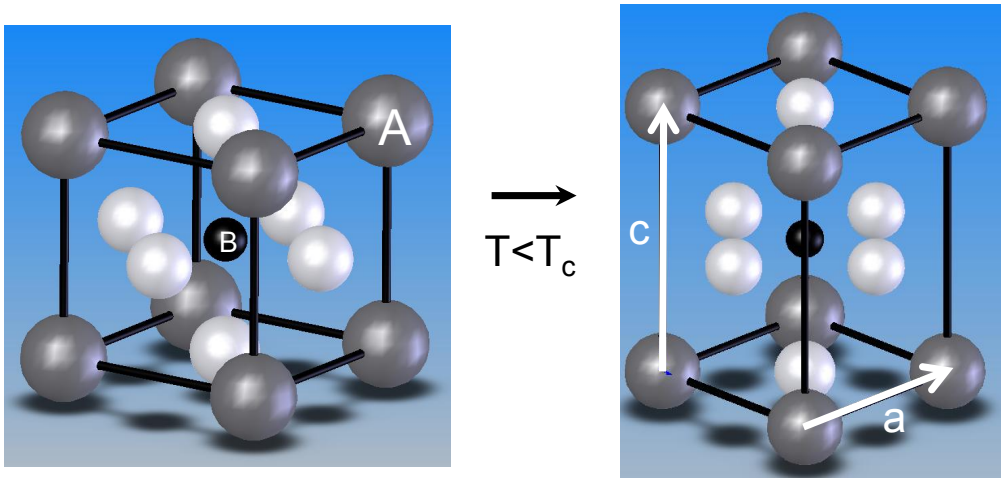

Figure 2.2. The ABO_3 perovskite unit cell is shown above (left) and below (right) the Curie temperature. The A atom is shown in the center, the B atoms are shown on 8 corner sites, and the oxygen atoms are shown on the face-centered sites.

From an energetics standpoint, Uchino gives the energy of the spontaneous dipole for N atoms per unit volume as [116]:

$$E_{dipole} = -\frac{N\alpha\gamma^2}{9\epsilon_0^2}\vec{\mathcal{P}}^2 \tag{2.1}$$

where α is the ionic polarizability of the ion, γ is the Lorentz factor, ϵ_0 is permittivity of vacuum, and $\mathcal{P}$ is the surrounding polarization. In addition, the elastic energy associated with ion displacement from its equilibrium position, $\vec{u}$, is given by:

$$E_{elastic} = N\left[\left(\frac{k}{2}\right)\vec{u}^2 + \left(\frac{k'}{2}\right)\vec{u}^4\right] \tag{2.2}$$

where k and k' represent the two spring constants associated with the energy between ions within a unit cell and between different unit cells, respectively. By assuming $\mathcal{P} = Nq\vec{u}$, where q is electric charge, we arrive at:

$$E_{total} = E_{dipole} + E_{elastic} = \left[\left(\frac{k}{2Nq^2}\right) - \left(\frac{N\alpha\gamma^2}{9\epsilon_0^2}\right)\right]\vec{\mathcal{P}}^2 + \left[\frac{k'}{4N^3q^4}\right]\vec{\mathcal{P}}^4 \tag{2.3}$$

This says that if the elastic energy within the crystal is greater than the dipole-dipole interactions, then there is no spontaneous polarization, $T > T_c$. If the converse is true, then there will be a spontaneous polarization, $T < T_c$.

2.3 Landau-Ginsburg Theory of Ferroelectrics

One analytic method of formalizing the second-order phase transition that occurs upon cooling a ferroelectric below its Curie temperature is to use the Landau Theory of phase transitions. This theory, which was developed by the Nobel Prize winning physicist Lev Landau, represents the free energy of a crystal as a phenomenological expression based on the order parameter, Ψ, of the total polarization. The generalized expression for the Landau free energy of the system, $\mathcal{F}$, is given by [112]:

$$\mathcal{F} = \mathcal{F}_0 + \frac{1}{2}\alpha\Psi^2 + \frac{1}{4}\beta\Psi^4 + \frac{1}{2}\delta\left(\vec{\nabla}\Psi\right)^2 - \vec{E}\Psi \tag{2.4}$$

Here, α and β are temperature dependent coefficients, and δ represents a restoring force which limits the minimum size of ferroelectric domains. This representation, which neglects terms higher than fourth order, and includes a term for polarization gradients, $\frac{1}{2}\delta\left(\vec{\nabla}\Psi\right)^2$, as well as an applied electric field, $-\vec{E}\Psi$. Due to the fact that the energy must be invariant under polarization reversal, the coefficients of all the odd powers of Ψ are zero.

For the case of ferroelectrics, the order parameter, Ψ, represents the polarization, $\mathcal{P}$, of the unit cell. Landau theory assumes that below the critical temperature, T_c, a spontaneous polarization will occur and that the components of $\mathcal{P}$ vary continuously across T_c. For the case of $BaTiO_3$, the change from a cubic to tetragonal unit cell will result in a spontaneous polarization and can be written as [56]:

$$\begin{aligned}\mathcal{F} = \mathcal{F}_0 + \tfrac{1}{2}\left(\alpha_z\mathcal{P}_z^2 + \left[\mathcal{P}_x^2 + \mathcal{P}_y^2\right]\right)\alpha_{xy} \\ +\tfrac{1}{4}\left(\beta_1\mathcal{P}_z^4 + \beta_2\left[\mathcal{P}_x^2 + \mathcal{P}_y^2\right]^2 + \beta_3\left[\mathcal{P}_x^2 - \mathcal{P}_y^2\right]^2 + \beta_4\left[\mathcal{P}_x^2\mathcal{P}_y^2\right] + \beta_5\mathcal{P}_z^2\left[\mathcal{P}_x^2 + \mathcal{P}_y^2\right]\right) \\ +\tfrac{1}{2}\delta\left(\vec{\nabla}\Psi\right)^2 - \vec{E}\Psi\end{aligned} \tag{2.5}$$

For simplicity, we will assume that the spontaneous polarization is in the $\pm\mathcal{P}_z$ direction. In this

case, the Landau free energy of the crystal is given by:

$$\mathcal{F} = \mathcal{F}_0 + \frac{1}{2}\alpha\mathcal{P}_z^2 + \frac{1}{4}\beta_1\mathcal{P}_z^4 \tag{2.6}$$

and the equilibrium polarization of the crystal below the critical temperature is found by:

$$\frac{\partial\mathcal{F}}{\partial\mathcal{P}} = 0 = \alpha\mathcal{P} + \beta\mathcal{P}^3 = \mathcal{P}\left(\alpha + \beta\mathcal{P}^2\right) \tag{2.7}$$

which has the solutions:

$$\mathcal{P}_0 = 0, \pm\sqrt{\frac{-\alpha}{\beta}} \tag{2.8}$$

Here we let $\alpha = \alpha_0(\mathrm{T} - \mathrm{T}_c)$ where $\alpha_0 = \frac{C}{\epsilon_0}$. This gives the final form of the spontaneous polarization as:

$$\mathcal{P}_0 = 0, \pm\sqrt{\frac{\alpha_0\left(T_c - T\right)}{\beta}} \tag{2.9}$$

From this we can see that above T_c, when the material is paraelectric, there are no real solutions for $\mathcal{P}$, and below T_c there are two minima which correspond to the two-fold degeneracy in $\mathcal{P}$. For the case of the tetragonal unit cell of $BaTiO_3$, this corresponds to the $\pm\mathcal{P}_z$ polarization. Also, for the fourth order expansion, we require that $\beta > 0$ to ensure real solutions to $\mathcal{P}$ for $\mathrm{T} < \mathrm{T}_c$. We also note here that $\mathcal{P} \sim |\mathrm{T} - \mathrm{T}_c|^\beta$, and as a result, the critical exponent $\beta = \frac{1}{2}$.

A plot of this is shown in Figure 2.3. Here, $\pm\mathcal{P}_z$ can be seen below the x-axis and no spontaneous polarization can be seen in the curve representing $\mathrm{T} > \mathrm{T}_c$. Additionally, $\Delta = \alpha\Psi^2$ is shown below the x-axis which represents the energy penalty for wide domain walls within the ferroelectric.

Although it is beyond the scope of this thesis, at T_c this formalism for ferroelectrics can be used to analyze: the absence of any latent heat; a discontinuity in the specific heat; and a divergence in the susceptibility [112].

2.4 Electro-optic Effects

The response of any crystal to an external field will depend strongly on the frequency of that field. With visible light, the frequency is $\sim$ 430 - 750 THz and as a result, only the electrons within a solid can respond. For electro-optic materials, the application of an external electric field will induce a displacement of the ion cores within the material. This results in a change in the electron density distribution throughout the material, and as a result, a change in the materials index of

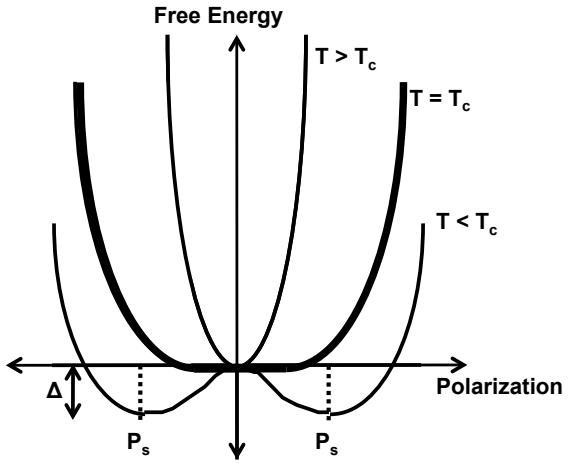

Figure 2.3. Landau Free Energy of the crystal as a function of polarization at three temperatures: T > T_c which exhibits no spontaneous polarization, T = T_c, and T < T_c which has a two-fold solution.

refraction. For the case of an electric field applied in the $\hat{z}$ direction, the redistribution of the ions within the lattice would produce an elongation in the $\hat{z}$ direction and a corresponding contraction in the $\hat{x}$ and $\hat{y}$ directions. As a result, the electron density (and index or refraction) would decrease in the $\hat{z}$ direction and would increase in the $\hat{x}$ and $\hat{y}$ directions.

As discussed in Appendix B, we know that the index within a material is a second-rank tensor which is given by [116]:

$$\frac{1}{n_{ij}^2(E)} - \frac{1}{n_{ij}^2(0)} = \sum_k r_{ijk} E_k + \sum_{kl} R_{ijkl} E_k E_l \tag{2.10}$$

where $n_{ij}(E)$ and $n_{ij}(0)$ are the indicies of refraction with and without an applied electric field, respectively. r_{ijk} is the Pockels coefficient which represents the linear electro-optic effect, and R_{ijkl} is the Kerr coefficient which represents the quadratic electro-optic effect.

As an example, the ABO_3 perovskites discussed in Section 2.2.2 (Figure 2.1) show that in their paraelectric phase, these materials belong to the m3m symmetry group. As a result, the Kerr

coefficients for this crystal structure are given by [116]:

$$\begin{bmatrix} R_{11} & R_{12} & R_{12} & 0 & 0 & 0 \\ R_{12} & R_{11} & R_{12} & 0 & 0 & 0 \\ R_{12} & R_{12} & R_{11} & 0 & 0 & 0 \\ 0 & 0 & 0 & R_{44} & 0 & 0 \\ 0 & 0 & 0 & 0 & R_{44} & 0 \\ 0 & 0 & 0 & 0 & 0 & R_{44} \end{bmatrix} \tag{2.11}$$

2.5 Piezoresponse Force Microscopy

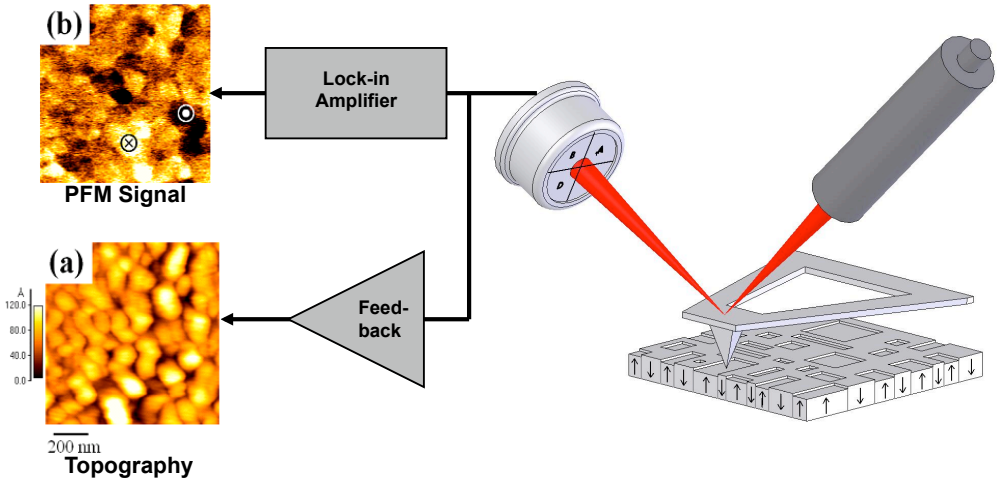

Figure 2.4. A schematic of a typical PFM setup is shown. Both topography (a) and piezoresponse (b) as a function of position on the sample are shown.

One method of investigating the behavior of piezoelectrics that will be utilized in Chapter 3 is Piezoresponse Force Microscopy (PFM). This technique utilizes a standard atomic force microscope (AFM) with a conductive scanning tip. The tip is rastered across the sample surface in a series of line scans which are compiled to produce a topological image of the surface of the sample. At the same time, a lock-in amplifier is used to apply a DC offset to the tip as well as an AC voltage (traditionally from 1 - 5 kHz). The applied electric fields cause the piezoelectric material to expand and contract with the AC voltage and this time-dependent response (whose frequency is that of the drive signal) is separated from the rest of the topological data using the same lock-in amplifier,

Figure 2.4. This is necessary because the piezoresponse signal from the sample is usually near the lower detection limit of the AFM and as a result, the topography will dominate the output signal. This is especially true with rough samples which might also have surface oscillation frequencies which are similar to those of the piezoresponse!

In general, the piezoresponse from the sample is given by:

$$\Delta z = -d^* V \tag{2.12}$$

where d^* is the piezoelectric coefficient of the material and is > 0 for positive domains, Δz is the change in height of the sample from the converse piezoelectric effect, and V is the applied voltage. Including the AC voltage gives:

$$V = V_{DC} + V_{AC}\sin(\omega t) \tag{2.13}$$

$$\Delta z = d^*_{33} V_{AC}\sin(\omega t + \Phi) \begin{cases} \Phi = \pi \text{ for } P_z > 0 \\ \Phi = 0 \text{ for } P_z < 0 \end{cases} \tag{2.14a}$$

where $P_z > 0$ indicates that there is a spontaneous positive polarization at the crystal/tip interface, ω is the drive frequency of the AC voltage, and d^*_{33} is the constrained out-of-plane piezoelectric coefficient. This value is less that d_{33} for an individual unit cell because of the fact that it is constrained by the film around it. The two constants are related by the compliance of the film "s_{ij}" and the shear components of the piezoresponse:

$$d^*_{33} = d_{33} - \frac{2d_{31}s_{12}}{s_{11} + s_{12}} \tag{2.15}$$

2.6 Ion Implantation Induced Layer Transfer

To fabricate single crystals of the ferroelectrics studied in this thesis, we utilize a technique known as ion implantation induced layer transfer (or layer transfer for short). The process consists of four main steps. The first, which will be discussed in Chapter 3, is ion implantation. This step consists of sending high energy H^+ ions into a single crystal of the material to be transferred. Often times, the material is also co-implanted with either He^+ or B^+. The depth of implantation is determined by the energy of implantation and a gaussian distribution of the implanted depths is obtained. If

two ions are co-implanted, the energies of implantations should be tuned so that the peaks of the implantation distributions overlap, and these calculations are done using Stopping and Range of Ions in Matter (SRIM) software [6].

Upon implantation of the single crystal sample, the surfaces of both the implanted sample as well as the substrate to which it will be bonded are cleaned and "activated" using a plasma treatment process. The effectiveness of the plasma activation can be determined using contact angle measurements of the "as treated" surface with a microsyringe imaging system, Figure 2.5.

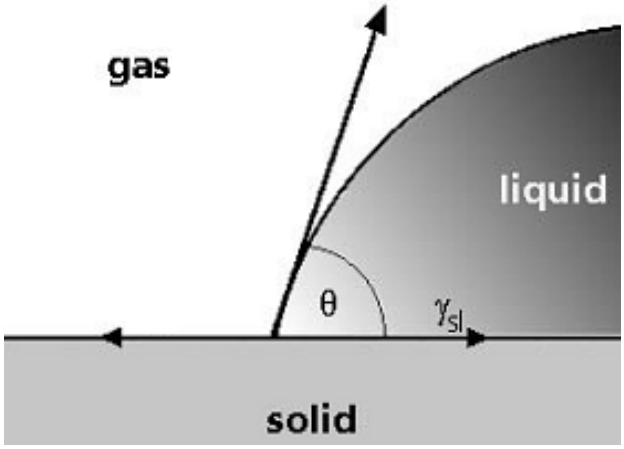

Figure 2.5. Typical solid-liquid-gas contact angle schematic used in determining the effectiveness of plasma treatment before wafer bonding.

After surface treatment of the implanted sample and substrate are complete, the two surfaces are brought in contact under high temperature and pressure. At high temperature, the implanted species preferentially diffuse through the implanted crystal along the plane of implantation. This process induces the formation of gas voids. Provided the crystal is under an acceptable amount of compressive stress during this process (Chapter 4), the edges of these voids grow along the plane of implantation, join with other voids, and eventually cleave off a thin film single crystal layer of the implanted material. A schematic of this process is shown in Figure 2.6.

Optimizing each of the different steps in Figure 2.6 is non-trivial and Chapters 2, 3, and 4 will discuss research that was done to produce a coherent, layer transferred film. As difficult as this process is, there are significant benefits to using this method of fabrication over other

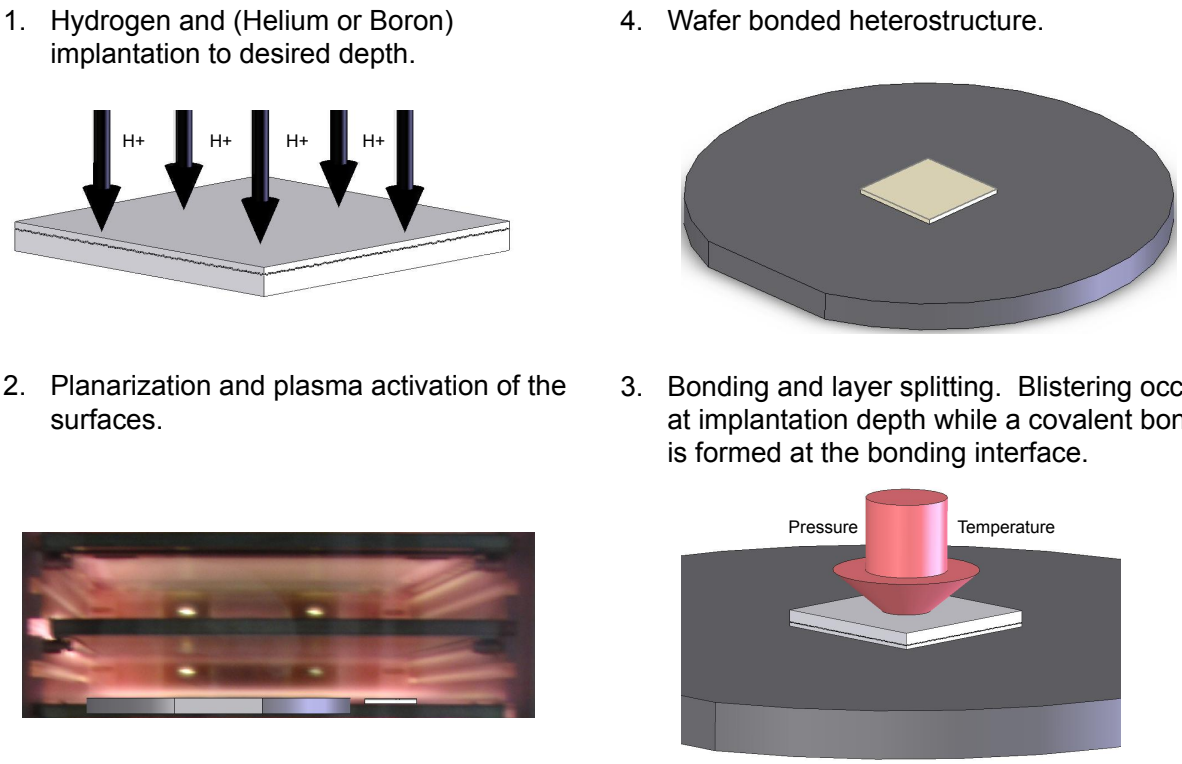

Figure 2.6. A schematic process flow of the layer transfer process.

techniques. Fabrication methods fall into two broad categories, bottom up and top down. Bottom up fabrication involves the deposition of successive layers. Using lithography and etching steps after each deposition, your structure is fabricated from the "bottom up". This method is extremely flexible and allows the integration of a wide variety of materials. The drawback to this technique is that the films will either be amorphous or polycrystalline. On the other hand, top down processing uses various etch steps to drill into a substrate and fabricate your structure from the "top down". Provided you start with a single crystal substrate, this method has the benefit of producing single crystal structures; however, this technique is not nearly as flexible in terms of integrating different materials and structures. Ideally, ion implantation induced layer transfer would combine the best of both worlds and produce single crystal thin films using a bottom approach.